

New constraint on the existence of the $\mu^+ \rightarrow e^+\gamma$ decay

J. Adam,^{1,2} X. Bai,³ A. M. Baldini,⁴ E. Baracchini,^{3,5,6} C. Bemporad^{ab,4} G. Boca^{ab,7} P. W. Cattaneo^{a,7}
G. Cavoto^{a,8} F. Cei^{ab,4} C. Cerri^{a,4} A. de Bari^{ab,7} M. De Gerone^{ab,9} T. Doke,¹⁰ S. Dussoni^{a,4} J. Egger,¹
Y. Fujii,³ L. Galli^{a,1,4} F. Gatti^{ab,9} B. Golden,⁶ M. Grassi^{a,4} A. Graziosi^{a,8} D. N. Grigoriev,^{11,12} T. Haruyama,⁵
M. Hildebrandt,¹ Y. Hisamatsu,³ F. Ignatov,¹¹ T. Iwamoto,³ D. Kaneko,³ P.-R. Kettle,¹ B. I. Khazin,¹¹
N. Khomotov,¹¹ O. Kiselev,¹ A. Korenchenko,¹³ N. Kravchuk,¹³ G. Lim,⁶ A. Maki,⁵ S. Mihara,⁵ W. Molzon,⁶
T. Mori,³ D. Mzavia,¹³ R. Nardò,⁷ H. Natori,^{5,3,1} D. Nicolò^{ab,4} H. Nishiguchi,⁵ Y. Nishimura,³ W. Ootani,³
M. Panareo^{ab,14} A. Papa,¹ G. Piredda^{a,8} A. Popov,¹¹ F. Renga^{a,8,1} E. Ripiccini^{ab,8} S. Ritt,¹ M. Rossella^{a,7}
R. Sawada,³ F. Sergiampietri^{a,4} G. Signorelli^{a,4} S. Suzuki,¹⁰ F. Tenchini^{ab,4} C. Topchyan,⁶ Y. Uchiyama,^{3,1}
C. Voena^{a,8} F. Xiao,⁶ S. Yamada,⁵ A. Yamamoto,⁵ S. Yamashita,³ Z. You,⁶ Yu. V. Yudin,¹¹ and D. Zanello^{a8}

(MEG Collaboration)

¹Paul Scherrer Institut PSI, CH-5232 Villigen, Switzerland

²Swiss Federal Institute of Technology ETH, CH-8093 Zürich, Switzerland

³ICEPP, The University of Tokyo 7-3-1 Hongo, Bunkyo-ku, Tokyo 113-0033, Japan

⁴INFN Sezione di Pisa^a; Dipartimento di Fisica^b dell'Università, Largo B. Pontecorvo 3, 56127 Pisa, Italy

⁵KEK, High Energy Accelerator Research Organization 1-1 Oho, Tsukuba, Ibaraki 305-0801, Japan

⁶University of California, Irvine, CA 92697, USA

⁷INFN Sezione di Pavia^a; Dipartimento di Fisica^b dell'Università, Via Bassi 6, 27100 Pavia, Italy

⁸INFN Sezione di Roma^a; Dipartimento di Fisica^b dell'Università "Sapienza", Piazzale A. Moro, 00185 Roma, Italy

⁹INFN Sezione di Genova^a; Dipartimento di Fisica^b dell'Università, Via Dodecaneso 33, 16146 Genova, Italy

¹⁰Research Institute for Science and Engineering, Waseda University, 3-4-1 Okubo, Shinjuku-ku, Tokyo 169-8555, Japan

¹¹Budker Institute of Nuclear Physics, 630090 Novosibirsk, Russia

¹²Novosibirsk State Technical University, 630092, Novosibirsk, Russia

¹³Joint Institute for Nuclear Research, 141980, Dubna, Russia

¹⁴INFN Sezione di Lecce^a; Dipartimento di Fisica^b dell'Università, Via per Arnesano, 73100 Lecce, Italy

(Dated: October 3, 2018)

The analysis of a combined dataset, totaling 3.6×10^{14} stopped muons on target, in the search for the lepton flavour violating decay $\mu^+ \rightarrow e^+\gamma$ is presented. The data collected by the MEG experiment at the Paul Scherrer Institut show no excess of events compared to background expectations and yield a new upper limit on the branching ratio of this decay of 5.7×10^{-13} (90% confidence level). This represents a four times more stringent limit than the previous world best limit set by MEG.

PACS numbers: 13.35.Bv; 11.30.Hv; 11.30.Pb; 12.10.Dm

The lepton flavour violating $\mu^+ \rightarrow e^+\gamma$ decay is predicted to have an unobservable low rate within the Standard Model of elementary particle physics (SM), despite the existence of neutrino oscillations [1]. Conversely, the majority of new physics models [2–5] Beyond SM (BSM), particularly in view of the recent measurements of a large θ_{13} at reactor [6–8] and accelerator [9] experiments, predict measurable rates for this decay. An observation of the $\mu^+ \rightarrow e^+\gamma$ decay would therefore represent an unambiguous sign of BSM physics, whereas improvements in the branching ratio upper limit constitute significant constraints on the parameter space, complementary to those obtainable at high energy colliders.

The present best upper limit on the $\mu^+ \rightarrow e^+\gamma$ decay branching ratio \mathcal{B} ($\mathcal{B} < 2.4 \times 10^{-12}$ at 90% C.L.) was set by the MEG experiment [10] with an analysis of the data taken in the years 2009–2010, for a total number of 1.75×10^{14} positive muons stopped on target.

In this paper we present an updated analysis of the 2009–2010 data sample, based on recently improved algorithms for the reconstruction of positrons and photons

together with the analysis of the data sample collected in 2011 with a beam intensity of $3 \times 10^7 \mu^+/\text{s}$, which corresponds to 1.85×10^{14} stopped muons on target. Furthermore the combined analysis of the full 2009–2011 statistics is presented.

The signature of the signal event is given by a back-to-back, monoenergetic, time coincident photon-positron pair from the two body $\mu^+ \rightarrow e^+\gamma$ decay. In each event, positron and photon candidates are described by five observables: the photon and positron energies (E_γ , E_e), their relative directions ($\theta_{e\gamma}$, $\phi_{e\gamma}$) [11] and emission time ($t_{e\gamma}$). Our analysis is based on a maximum likelihood technique applied in the analysis region defined by $48 < E_\gamma < 58$ MeV, $50 < E_e < 56$ MeV, $|t_{e\gamma}| < 0.7$ ns, $|\theta_{e\gamma}| < 50$ mrad and $|\phi_{e\gamma}| < 50$ mrad, which is described in detail in [10]. We call “time sidebands” the regions in the variable space defined by $1 < |t_{e\gamma}| < 4$ ns, “ E_γ -sideband” that defined by $40 < E_\gamma < 48$ MeV and “angle sidebands” those defined by $50 < |\phi_{e\gamma}| < 150$ mrad or $50 < |\theta_{e\gamma}| < 150$ mrad.

The background has two components, one coming

from the Radiative Muon Decay $\mu^+ \rightarrow e^+ \nu \bar{\nu} \gamma$ (RMD) and one from the accidental superposition of energetic positrons from the standard muon Michel decay with photons from RMD, positron-electron annihilation-in-flight or bremsstrahlung. At the MEG data taking rate, 93% of events with $E_\gamma > 48$ MeV are from the ACCidental background (ACC).

The MEG detector is described in detail elsewhere [12]. It is comprised of a positron spectrometer formed by a set of Drift CHambers (DCH) and scintillation Timing Counters (TC), located inside a superconducting solenoid with a gradient magnetic field along the beam axis, and a photon detector, located outside of the solenoid, made up of a homogeneous volume (900 ℓ) of Liquid Xenon (LXe) viewed by 846 UV-sensitive photomultiplier tubes (PMTs) submerged in the liquid.

The MEG detector response, resolutions and stability are constantly monitored and calibrated by means of a multi-element calibration system [10, 12], which was recently complemented with a new method based on the Mott scattering of a monochromatic positron beam. Two important hardware improvements were introduced in 2011, one in the $\pi^- p \rightarrow \pi^0 n$ Charge EXchange reaction (CEX) calibration by replacing the NaI detector, used to define the back-to-back coincidence with the LXe detector when observing the two photons from π^0 decay, with a higher resolution BGO array detector, the other in the optical survey technique for the DCH by using a laser tracker and prismatic corner cube reflectors mounted on the DCH modules.

In 2011 the DAQ efficiency, being the product of DAQ live time fraction and trigger efficiency to select signal event, was at the level of 96%. An improvement from 72% in 2010 is due to a new multiple buffer read out scheme, which guarantees a 99% live time fraction with a less constrained event selection, thus allowing a 97% signal trigger efficiency [13].

The positron track is reconstructed by combining its measured positions at each DCH layer (hit) in the spectrometer. Longitudinal (along the muon beam direction) z -positions are derived from signals induced on the segmented DCH cathodes. Electromagnetic noise has been the main source of degradation of the z -resolution during all the data-taking periods and a new reconstruction algorithm based on a fast Fourier transform filtering technique has been applied to mitigate such effect, yielding an up to $\sim 10\%$ improvement in angular resolution. Internal alignment of the DCH layers is obtained by tracking cosmic ray muons with the magnet off and using an optical survey, as described in [10].

The positron kinematic variables are extracted by means of a Kalman filter track fitting technique [14, 15]. This algorithm has been completely revised for this analysis to include a better model for the hits and the track itself, based on the GEANE package [16, 17]. An improved model for the detector material, accounting for multiple

scattering and energy loss as well as a detailed map of the non-uniform magnetic field, measured with a 0.2% precision has also been included. The fitted positron track is propagated to the TC allowing an iterative refinement of the hits with the positron time measurement.

The track fit yields a covariance matrix for the parameters, resulting in very good agreement with the measured resolutions, which are extracted from a sample of tracks with two full turns in the DCH, by comparing the track parameters determined independently for each turn at an intermediate plane. Consequently a per-track error is determined which allows us to follow the variable DCH performance during the data-taking period and is taken into account in the maximum likelihood analysis.

The average hit multiplicity for a track is about 10 and only tracks with at least 7 hits and either one or two turns in the spectrometer are retained for the analysis. Additional quality requirements on the χ^2 fit value and parameter uncertainties are applied to select only one positron per event. The overall improvement in positron reconstruction with respect to the previous data analysis is clearly visible in Fig.1 (top) where the reconstructed positron energy near the kinematic edge of the Michel decay spectrum shows a reduced tail. The energy resolution is evaluated by fitting the kinematic edge and it is well described by the sum of three Gaussian curves with a resolution of $\sigma_{E_e} = 305$ keV for the core component (85%).

The resolution in the azimuthal angle of the positron when it leaves the target, ϕ_e , has a dependence on ϕ_e itself with a minimum at $\phi_e = 0$, where it is measured by the two-turn method after correcting for all known correlations to be $\sigma_{\phi_e} = 7.5$ (7.0) mrad [18]. Similarly, the resolution in the polar angle, θ_e , is measured to be $\sigma_{\theta_e} = 10.6$ (10.0) mrad. The decay vertex coordinates and the positron direction at the vertex are determined by extrapolating the reconstructed track back to the target. The resolutions on the decay vertex coordinates are also determined by the two-turn method and are described by a Gaussian curve with $\sigma_z = 1.9$ (1.5) mm and, in the vertical direction, by the sum of two Gaussian curves with $\sigma_y = 1.3$ (1.2) mm for the core component (85%).

The LXe detector uses the xenon scintillation light to measure the total energy released by the photon, the position and time of its first interaction. The three-dimensional photon conversion point is reconstructed by using the distribution of the number of scintillation photons detected by the PMTs near the incident position. The photon direction is defined by the line connecting the decay vertex to the photon conversion point in the LXe detector. The reconstruction of the photon energy is based on the sum of the scintillation light detected by all PMTs. Monochromatic 55 MeV photons from π^0 decays are used to determine the absolute energy scale. The photon conversion time is reconstructed by combining the leading edge times of the PMT waveforms.

It is important to identify and unfold photon pile-up events at high muon rates since at $3 \times 10^7 \mu^+ / s$ beam rate, around 15% of triggered events suffer from pile-up. For the previously published analyses, photon pile-up events were identified topologically by the pattern of PMT light distribution and temporally by the leading edge time distribution in the time reconstruction, without the use of detailed waveform information. In addition to these methods, a new algorithm, analyzing waveforms after summing up all channels at the end of the full chain of photon reconstruction, was developed. It enables the efficient identification and removal of pile-up photons by using template waveforms. Consequently the charge integration window for the energy estimate is re-adjusted, resulting in a better energy reconstruction. This improvement is shown in Fig. 1 (bottom) where we compare the photon energy spectra obtained with different pile-up elimination algorithms. The reduced tail in the high energy region is clearly visible. The efficiency of photon reconstruction is improved from 59% to 63% due to the new algorithm.

The performance of the position reconstruction is evaluated by a Monte Carlo simulation, resulting in resolutions of 5 mm on the photon entrance face, and 6 mm along the radial depth from the entrance face. This is validated in CEX runs by placing lead slit collimators in front of the LXe detector. The timing and the energy resolutions are evaluated using two simultaneous back-to-back photons from π^0 decay. The LXe timing resolution is found to be $\sigma_{t_\gamma} = 67$ ps at the signal energy. The position-dependent energy resolutions are measured in the CEX data and the average energy resolution extracted from a Gaussian fit to the high energy side of the spectrum is evaluated to be 1.7% (1.9%) and 2.4% (2.4%) for radial depths larger and smaller than 2 cm respectively. These position-dependent energy resolutions are incorporated into the likelihood analysis.

The resolutions of the relative directions ($\theta_{e\gamma}$, $\phi_{e\gamma}$) are derived by combining the relevant resolutions of positrons and photons discussed above. The results are 16.2 (15.7) mrad for $\theta_{e\gamma}$ and 8.9 (9.0) mrad for $\phi_{e\gamma}$ after correcting for all known correlations. The relative time $t_{e\gamma}$ is derived from the time measurements, one in the LXe detector and the other in the TC, after correcting for the lengths of the particle flight-paths. The associated resolutions at the signal energy are 127 (135) ps, evaluated from the RMD peak observed in the E_γ -sideband; a small correction takes into account the E_γ -dependence measured in the CEX calibration runs. The position of the RMD-peak corresponding to $t_{e\gamma} = 0$ was monitored constantly during the physics data-taking period and found to be stable to within 15 ps.

A blind analysis procedure is applied only to the new dataset in 2011 by masking a region of $48 < E_\gamma < 58$ MeV and $|t_{e\gamma}| < 1$ ns until the Probability Density Functions (PDFs) for the likelihood function are finalized. For all

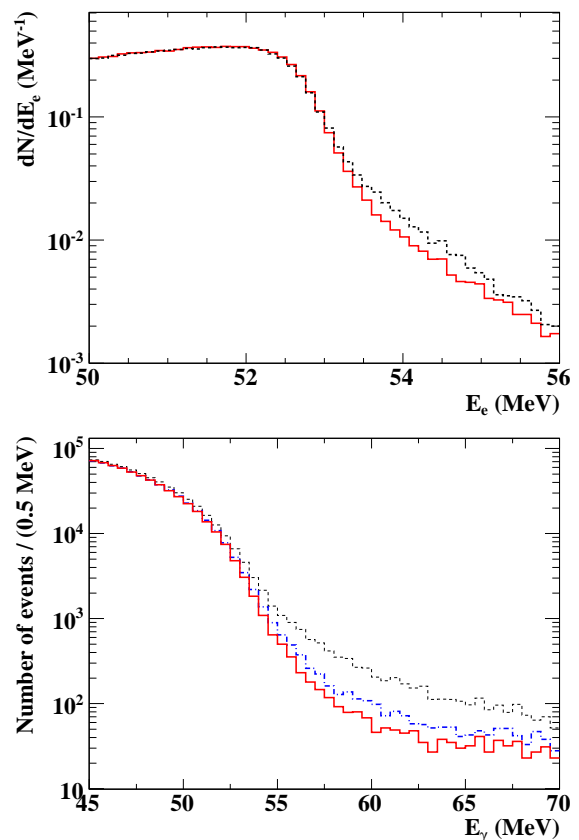


FIG. 1: (Top) The Michel positron spectrum in the same dataset in the time sidebands with the old (black dashed line) and the new (red solid line) track reconstruction code. (Bottom) The photon background spectra from the time sidebands of the muon data in 2010 with different pile-up elimination algorithms. Black dots: no pile-up elimination; blue dot-dashed: previous algorithm; red solid: new algorithm.

the datasets including 2009–2010 data the background studies and the extraction of the PDFs are carried out in the time and angle sidebands. The maximum likelihood fit is performed in order to estimate the number of signal, RMD and ACC events in the analysis region. The definition of the likelihood function is described in detail in [10]. All PDFs as a function of the observables are extracted from the data. Different resolutions and correlations are used in the PDFs on an event-by-event basis. The dependence on the photon interaction position and the quality of the positron tracking has already been incorporated into the previous analysis, while in the new analysis a per-event error matrix for the positron observables, estimated by the new Kalman filter, has been introduced into the PDFs. The sensitivity is improved by about 10% in the new analysis with the positron per-event error matrix. An analysis with constant PDFs is also performed as a crosscheck, showing consistent re-

sults. The confidence interval for the number of signal events is calculated by a frequentist method with a profile likelihood-ratio ordering [10, 19, 20], where the numbers of RMD and ACC events are treated as nuisance parameters.

To translate the estimated number of signal events into a signal branching ratio two independent normalization methods are used, either counting the number of Michel positrons selected with a dedicated trigger or the number of RMD events observed in the muon data. Their combination leads to a 4% uncertainty in the branching ratio estimate. The increased reconstruction efficiency of the new algorithms results in a 14% larger data sample for the $\mu^+ \rightarrow e^+\gamma$ search, as estimated with both normalization methods, with both positron and photon new algorithms contributing equally.

The systematic uncertainties on the PDF parameters and on the normalization are taken into account in the calculation of the confidence intervals by fluctuating the PDFs by the amount of the uncertainties. In total they produce a 1% effect on the observed upper limit, with the majority of the contribution coming from the angular PDFs.

The sensitivity (\mathcal{S}_{90}) is estimated as the median of the distribution of the branching ratio upper limits at 90% C.L., calculated over an ensemble of pseudo-experiments, randomly generated according to the PDFs based on a null signal hypothesis, with the rates of ACC and RMD evaluated from the sidebands. The sensitivities have been so evaluated for the 2009–2010 combined data, the 2011 data alone and the 2009–2011 combined data sample, and are reported in Table I. Likelihood analyses are also performed in fictitious analysis regions in both the time- and angle-sidebands, getting upper limits all in good agreement with the \mathcal{S}_{90} 's.

Figure 2 shows the event distributions in the (E_e, E_γ) - and $(\cos \Theta_{e\gamma}, t_{e\gamma})$ -planes for the combined 2009–2011 dataset, where $\Theta_{e\gamma}$ is the opening angle between positron and photon, together with the contours of the averaged signal PDFs.

The observed profile likelihood ratios as a function of the branching ratio are shown in Fig. 3. The best \mathcal{B} estimates, upper limits at 90% C.L. (\mathcal{B}_{90}) and \mathcal{S}_{90} for the combined 2009–2010 dataset, the 2011 data alone and the total 2009–2011 dataset are listed in Table I. The \mathcal{B}_{90} for the latter is 5.7×10^{-13} . As a quality check the maximum likelihood fit is repeated for the 2009–2011 dataset omitting the constraint on the number of background events. We obtain $N_{\text{RMD}} = 163 \pm 32$ and $N_{\text{ACC}} = 2411 \pm 57$, in good agreement with the expectations estimated from E_γ and time sidebands, $\langle N_{\text{RMD}} \rangle = 169 \pm 17$ and $\langle N_{\text{ACC}} \rangle = 2415 \pm 25$.

The reanalysis of the 2009–2010 dataset with new algorithms has led to variations in the values of the observables which are much smaller than the detector resolutions. The events observed with the highest signal-

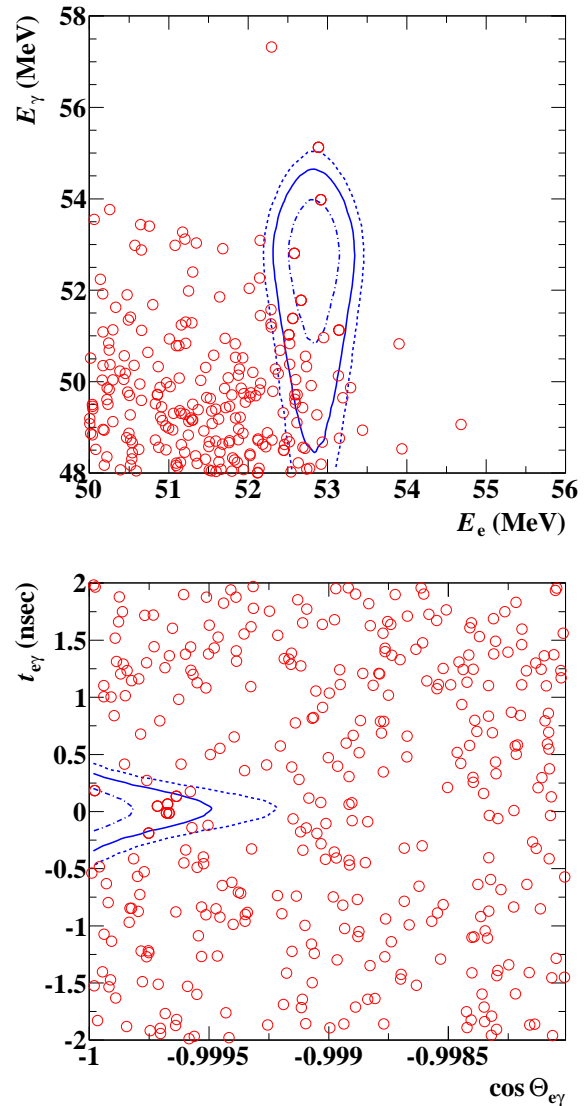


FIG. 2: Event distributions for the combined 2009–2011 dataset in the (E_e, E_γ) - and $(\cos \Theta_{e\gamma}, t_{e\gamma})$ -planes. In the top (bottom) panel, a selection of $|t_{e\gamma}| < 0.244$ ns and $\cos \Theta_{e\gamma} < -0.9996$ with 90% efficiency for each variable ($52.4 < E_e < 55$ MeV and $51 < E_\gamma < 55.5$ MeV with 90% and 74% efficiencies for E_e and E_γ , respectively) is applied. The signal PDF contours (1, 1.64 and 2 σ) are also shown.

likelihood in the previous analysis of the 2009–2010 dataset have also moved in the new analysis within the expected fluctuation and mostly have had their signal-likelihood slightly reduced. These small variations induce a change in \mathcal{B}_{fit} and \mathcal{B}_{90} for the same dataset. We have compared \mathcal{B}_{90} 's obtained with the new and old analyses for the same sample of simulated experiments and found that a change of \mathcal{B}_{90} equal to or larger than what we observe in the 2009–2010 dataset has a 31% probability of occurring. The upper limit obtained from the 2011 data only is more stringent than \mathcal{S}_{90} . This is, however,

TABLE I: Best fit values (\mathcal{B}_{fit} 's), branching ratios (\mathcal{B}_{90}) and sensitivities (\mathcal{S}_{90})

Dataset	$\mathcal{B}_{\text{fit}} \times 10^{12}$	$\mathcal{B}_{90} \times 10^{12}$	$\mathcal{S}_{90} \times 10^{12}$
2009–2010	0.09	1.3	1.3
2011	-0.35	0.67	1.1
2009–2011	-0.06	0.57	0.77

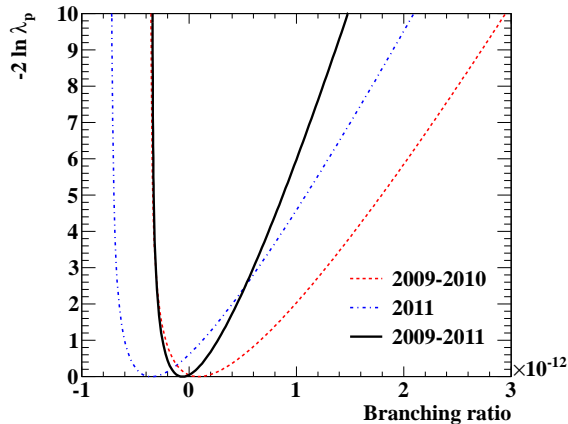


FIG. 3: Observed profile likelihood ratios (λ_p) as a function of the branching ratio for the 2009–2010 combined data, the 2011 data alone and the combined 2009–2011 data sample.

not considered unusual, since the probability to have \mathcal{B}_{90} equal or smaller than that observed in the 2011 data is calculated to be 24% with a sample of simulated experiments.

In conclusion the MEG experiment has so established the most stringent upper limit to date on the branching ratio of the $\mu^+ \rightarrow e^+\gamma$ decay, $\mathcal{B} < 5.7 \times 10^{-13}$ at 90% C.L. using data collected between 2009 and 2011, which improves the previous best upper limit by a factor of four. Further data have also been acquired in 2012 with an additional three-month run scheduled for 2013; the final number of stopped muons is expected to be almost twice that of the sample analyzed so far. Currently an upgrade

program is underway aiming at a sensitivity improvement of a further order of magnitude [21].

ACKNOWLEDGEMENTS

We are grateful for the support and cooperation provided by PSI as the host laboratory and to the technical and engineering staff of our institutes. This work is supported by SNF grant 137738 (CH), DOE DEFG02-91ER40679 (USA), INFN (Italy) and MEXT KAKENHI 22000004 (Japan). Partial support of the Italian Ministry of University and Research (MIUR) grant RBFR08XWGN is acknowledged.

-
- [1] S.T. Petcov, Sov. J. Nucl. Phys. **25** (1977) 340.
 - [2] R. Barbieri, L. Hall and A. Strumia, Nucl. Phys. B **445** (1995) 219.
 - [3] J. Hisano, D. Nomura and T. Yanagida, Phys. Lett. B **437** (1998) 351.
 - [4] M. Raidal *et al.*, Eur. Phys. J. C **57** (2008) 13.
 - [5] G. Blankenburg *et al.*, Eur. Phys. J. C **72** (2012) 2126.
 - [6] F.P. An *et al.*, Phys. Rev. Lett. **108** (2012) 171803.
 - [7] J.K. Ahn *et al.*, Phys. Rev. Lett. **108** (2012) 191802.
 - [8] Y. Abe *et al.*, arXiv:1301.2948 [hep-ex].
 - [9] K. Abe *et al.*, Phys. Rev. Lett. **107** (2011) 041801.
 - [10] J. Adam *et al.*, Phys. Rev. Lett. **107** (2011) 171801.
 - [11] $\theta_{e\gamma} = (\pi - \theta_e) - \theta_\gamma$ and $\phi_{e\gamma} = (\pi + \phi_e) - \phi_\gamma$, θ and ϕ being the polar angle and the azimuthal angle, respectively, taking the z -axis as the beam-axis.
 - [12] J. Adam *et al.*, Eur. Phys. J. C **73**(2013) 2365, arXiv:1303.2348 [physics.ins-det].
 - [13] L. Galli *et al.*, JINST **8** (2013) P01008.
 - [14] P. Billoir, Nucl. Instrum. Meth. A **225** (1984) 352.
 - [15] R. Frühwirth, Nucl. Instrum. Meth. A **262** (1987) 444.
 - [16] V. Innocente and E. Nagy, Nucl. Instrum. Meth. A **324** (1993) 297.
 - [17] A. Fontana *et al.* J. Phys. Conf. Ser. **119** (2008) 032018.
 - [18] From here on we will quote in parentheses the value in the 2009–2010 data when different from that in 2011.
 - [19] J. Beringer *et al.* (Particle Data Group), Phys. Rev. D **86** (2012) 010001.
 - [20] G. J. Feldman and R. D. Cousins, Phys. Rev. D **57** (1998) 3873.
 - [21] A. M. Baldini *et al.*, arXiv:1301.7225 [physics.ins-det].